RESEARCH

CrossMark

How well suited are current thermodynamic models to predict or interpret the composition of (Ba,Sr)SO$_4$ solid-solutions in geothermal scalings?

Frank Heberling[1]*, Dieter Schild[1], Detlev Degering[2] and Thorsten Schäfer[1]

*Correspondence:
Frank.Heberling@kit.edu
[1] Institute for Nuclear Waste
Disposal, Karlsruhe Institute
of Technology, PO Box 3640,
76021 Karlsruhe, Germany
Full list of author information
is available at the end of the
article

Abstract

In this study, we report results of the analysis of a particularly interesting scaling sample from the geothermal plant in Neustadt-Glewe in northern Germany, which contained 19% Galena (PbS) and 81% of a heterogeneous assemblage of (Ba,Sr)SO$_4$ crystals with varying compositions, $0.15 < X_{Ba} < 0.53$. A main fraction of the sample (~56%) has a barite content of $X_{Ba} \approx 0.32$. We try to relate the solid composition of the (Ba,Sr)SO$_4$ solid-solution to the conditions at the geothermal plant concerning temperature, pressure, and solution composition, and discuss it with respect to the challenges in modelling the composition of (Ba,Sr)SO$_4$ solid-solutions on the basis of thermodynamic mixing models. We note that considerable uncertainties are related to the description of (Ba,Sr)SO$_4$ formation by means of thermodynamic models. The scaling composition observed in this study would be in line with endmember solubilities as predicted by the PhreeqC-Pitzer database for 70 °C and an interaction parameter, $a_0 = 1.6$. According to such a model, the scaling heterogeneity would reflect bimodal precipitation behaviour due to various degrees of depletion of the brine with respect to $X(Ba)_{(aq)}$. Minor fluctuations in $X(Ba)_{(aq)}$: $0.0017 < X(Ba)_{(aq)} < 0.0042$ explain the full range of observed solid compositions. The choice especially of the interaction parameter seems to some extent arbitrary. This knowledge gap strongly limits the interpretation of (Ba,Sr)SO$_4$ compositions. Thus, it is not possible to distinguish between kinetic and thermodynamic effects on partitioning or to use the solid-solution composition to draw conclusions about the precipitation conditions (e.g. Temperature).

Background

(Ba,Sr)SO$_4$ solid-solutions range among the most important scaling minerals, not only in geothermal energy production, but generally in applications involving hydrothermal brines, e.g. including petroleum production [e.g. (Todd and Yuan 1990, 1992; Kühn et al. 1997)]. Besides the general difficulties related to scale formation, like blockage of pipes, related decrease of well productivity, and disturbances in geothermal plant operation, (Ba,Sr)SO$_4$ solid-solutions tend to incorporate natural radium isotopes (mainly ^{226}Ra and ^{228}Ra) to an extent that they may even become a radiological concern (Degering et al. 2011; IAEA 2003). Despite the relevance of (Ba,Sr)SO$_4$ solid-solutions as scaling

Heberling *et al. Geotherm Energy* (2017) 5:9

Page 2 of 16

mineral, it still needs to be considered a major challenge to predict their saturation state and to model their composition. Thus, it is not straightforward to predict where and in which composition $(Ba,Sr)SO_4$ solid-solutions will form in a geothermal water circuit. These challenges are related (1) to the conditions, which prevail in geothermal water: elevated temperature, pressure, and salinity, and (2) to the general difficulties related to modelling the formation of solid-solutions from aqueous solution (Prieto 2009; Prieto et al. 1997, 2016; Bruno 2007).

The endmembers of the $(Ba,Sr)SO_4$ solid-solution series, barite $(BaSO_4)$ and celestine $(SrSO_4)$ are isostructural and crystallize in a barite type crystal structure, space group Pbnm (Jacobsen et al. 1998). The thermodynamic properties of the endmembers and related aqueous species have been investigated in detail at standard conditions and at high temperature, pressure, and salinity (Monnin 1999; Blount 1977; Langmuir and Melchior 1985). Corresponding models are tabulated in thermodynamic databases [SIT. dat (Giffaut et al. 2014), Phreeqc.dat, Pitzer.dat (Appelo et al. 2014)] and are available for calculations with the geochemical modelling code PhreeqC (Parkhurst and Appelo 2013). As will be shown below, despite the available data pool, there is still considerable uncertainty even with respect to the solubility of the endmember phases. Concerning the mixing behaviour, thermodynamic parameters have been suggested based on the analysis of natural samples (e.g. Glynn 2000; Monnin and Cividini 2006) and theoretical calculations (Becker et al. 2000), and have been assessed experimentally [e.g. (Felmy et al. 1993)]. Based on natural samples it was suggested that barite and celestine form a slightly non-ideal regular solid-solution with the dimensionless interaction parameter a_0 in a range between $1.6 < a_0 < 2.34$ (Glynn 2000; Monnin and Cividini 2006). This parameter is thought to reproduce complete mixing in the solid-solution series. However, as already addressed by Monnin and Cividini (2006), the value of 2.34 is actually too high for this purpose, thus values in a range $1.6 < a_0 < 2.0$ may be considered reasonable from the perspective, that there should be no miscibility gap in this solid-solution series. Numerous problems are related to the determination of interaction parameters from experiments or natural samples (Prieto 2009; Prieto et al. 1997; Glynn 2000; Monnin and Cividini 2006). These may be overcome by calculating interaction parameters from the results of atomistic simulations. Based on such an approach Becker et al. (2000) and subsequently Prieto et al. (2000) report an elaborate model for the mixing properties of $(Ba,Sr)SO_4$ based on three symmetric interaction parameters (a_0, a_2, a_4). In contrast to previous assumptions, this model predicts a pronounced miscibility gap, which ranges from 2 to 98% at room temperature and becomes smaller with increasing temperature. Correspondingly, natural and experimental $(Ba,Sr)SO_4$ crystals with compositions inside the miscibility gap would reflect non-equilibrium partitioning, which, considering the kinetic controls affecting solid-solution precipitation, seems plausible as well.

Here we report results of the analysis of a particularly interesting scaling sample from the geothermal plant in Neustadt-Glewe in northern Germany, which contained Galena (PbS) and a heterogeneous assemblage of $(Ba,Sr)SO_4$ crystals with varying compositions. We try to relate the composition of the $(Ba,Sr)SO_4$ solid-solution to the conditions at the geothermal plant concerning temperature, pressure, and solution composition (Kühn et al. 1997; Seibt et al. 2005; Degering et al. 2009), and discuss it with respect to the challenges for modelling $(Ba,Sr)SO_4$ solid-solutions.

Heberling *et al. Geotherm Energy* (2017) 5:9

Page 3 of 16

Sample origin

The scaling sample originates from the geothermal plant in Neustadt-Glewe in the state of Mecklenburg-Vorpommern in northern Germany (Degering et al. 2011). The geothermal plant produces a hydrothermal brine (100 °C, 220 g/L salt content) from an upper Triassic sandstone (Rhätkeuper) in a depth of approximately 2300 m. A Geologic map highlighting the location of the geothermal plant is shown in the Additional file 1: Figure S1. Details on the geologic setting of the geothermal plant are given in (Seibt et al. 2005). Due to the relatively low temperature in the reservoir, the geothermal plant is mainly appropriate for heat production, and since 2011 it is exclusively used to produce heat. For this purpose, the brine is cooled down to 68–70 °C in an heat exchanger, before reinjection into the reservoir. The scaling sample originates from the cooler side of the heat exchanger, where the brine is close to reaching its final temperature of about 70 °C. For modelling purposes, we adopt the solution composition as given in Kühn et al. (1997): Na^+ 72.7 g/L, K^+ 828 mg/L, Ca^{2+} 8.7 g/L, Mg^{2+} 1.4 g/L, Sr^{2+} 450 mg/L, Ba^{2+} 5.3 mg/L, Cl^- 131.4 g/L, SO_4^{2-} 470 g/L, and pH 5.15 at reservoir conditions (230 bar and 100 °C), which corresponds to a total ionic strength of 4 mol/(kg water). A more complete analysis of the geothermal brine after Degering et al. (2009), which agrees within uncertainty with the composition used by Kühn et al. is presented in Additional file 1: Table S1. For the calculation of the aqueous mole fraction of barium [$X(Ba^{2+})_{(aq)}$, cf. below], we consider the full range of Sr^{2+} and Ba^{2+} concentrations reported by Degering et al. (2009) (445 ± 30 and 5.6 ± 0.4 mg/L for Sr^{2+} and Ba^{2+}, respectively). In the geothermal plant, 70 °C and 1 bar pressure is assumed. Note that pressures in a range as they might persist in the geothermal plant (usually higher than 1 bar, but below ~25 bar), have only a minor influence on the model results (i.e. the solubility products of barite and celestine). However, as the information about pressure effects on $(Ba,Sr)SO_4$ mixing is scarce, we decided to calculate assuming 1 bar. Note that all quantities reported as percent in this study refer to mol- or atom-percent.

Theoretical background

Before we start to discuss analytical methods and results, we will briefly lay out the most important concepts used to describe aqueous solution solid-solution systems. As we assume that the pressure at the point of scale formation (i.e. in the geothermal plant) is relatively low (<20 bar), we neglect any potential effect of pressure on mixing. For more detailed information, the reader is referred to text books or review articles (e.g. Prieto 2009; Prieto et al. 2016; Bruno 2007).

The composition of $(Ba,Sr)SO_4$ is usually described by the mole fractions (X) of barite and celestine, i.e. Ba^{2+} and Sr^{2+}, in the solid-solution. For example in a notation like: $Ba_X Sr_{(1-X)}SO_4$, X would denote the mole fraction of barite, X_{Ba} (=$1-X_{Ce}$, with X_{Ce} being the mole fraction of celestine). The free energy of a solid-solution is usually described relative to the free energy of a hypothetical mechanical mixture with equal composition, but without any molecular interactions between the components:

$$dG((Ba, Sr)SO_4)(X_{Ba}) = X_{Ba}\, dG^0(\text{barite}) + (1 - X_{Ba})\, dG^0(\text{celestine}) + dG^M(X_{Ba})$$

$$(1)$$

Heberling *et al. Geotherm Energy* (2017) 5:9

Page 4 of 16

Thus the molecular interactions between ions in the solid-solution are described by the free energy of mixing, dG^M. Local minima in the $dG^M (X_{Ba})$ curve mark the beginning and the end of a miscibility gap in the solid-solution series (cf. Fig. 5a, the beginning of the miscibility gap is marked as M1). The free energy of mixing again may be decomposed into an ideal free energy of mixing dG_{id}^M and an excess free energy of mixing dG^E,

$$dG^M = dG_{id}^M + dG^E. \tag{2}$$

For an ideal solid-solution $dG^E = 0$, by definition it has no enthalpy contribution to dG^M. Thus dG_{id}^M is fully governed by the conformational entropy, which in the case of random mixing in a binary solid-solution is given by:

$$dG_{id}^M(X_{Ba}) = RT \left[X_{Ba} \ln(X_{Ba}) + (1 - X_{Ba})\ln(1 - X_{Ba}) \right], \tag{3}$$

where R (=8.3145 J/mol/K) and T are the universal gas constant and the absolute temperature (K), respectively. This reflects that mixing in a solid-solution creates disorder and is therefore a favourable process concerning entropy. On the other hand side, for non-ideal solid-solutions, the incorporation of foreign ions into a host crystal structure usually involves a misfit of the ionic radii, and thus produces strain in the structure. This results in a positive enthalpy of mixing. Ordering in solid-solutions, on the other hand, results in states which are characterized by a decreased entropy. These types of effects are described by the excess free energy of mixing, dG^E. In order to model excess free energy of mixing, activity coefficients (*f*) for the endmember compounds in the solid-solution are introduced:

$$dG^E = RT \left(X_{Ba} \ln f_{Ba} + X_{Ce} \ln f_{Ce} \right). \tag{4}$$

Guggenheim (1937) proposed to describe dG^E in the form of an expansion series:

$$dG^E = X_{Ba} X_{Ce} RT \left[a_0 + a_1(X_{Ba} - X_{Ce}) + a_2(X_{Ba} - X_{Ce})^2 + \cdots \right] \tag{5}$$

The interaction parameters a_0, a_1, a_2,... are often called dimensionless Guggenheim parameters. In this study, we refer to such parameters, when we talk about interaction or mixing parameters. The functional form of dG^E (Eq. 5) allows to calculate solid-solution activity coefficients based on the two relations:

$$\ln f_{Ba} = \left[dG^E + X_{Ce} \, \partial dG^E / \partial X_{Ba} \right] / RT, \tag{6}$$

and

$$\ln f_{Ce} = \left[dG^E - X_{Ba} \, \partial dG^E / \partial X_{Ba} \right] / RT. \tag{7}$$

These equations are straightforward to solve, however, they become quite cumbersome when interaction parameters beyond a_2 are considered, as, e.g. in the present case for the model by Prieto et al. (2000). Solid-solution activity coefficients finally allow to relate the solid-solution composition to an aqueous solution composition in thermodynamic equilibrium with the mixed solid. Graphically this relation may be displayed in "Lippmann"- or "Rozeboom"- type phase diagrams. Lippmann diagrams are based on the concept of a total solubility product, $\Sigma\Pi$, which, for the present case, is defined as:

Heberling *et al. Geotherm Energy* (2017) 5:9

Page 5 of 16

$$\Sigma \Pi = K_{\text{Ba}} f_{\text{Ba}} X_{\text{Ba}} + K_{\text{Ce}} f_{\text{Ce}} X_{\text{Ce}}. \tag{8}$$

Here K_{Ba} and K_{Ce} are the solubility products of barite and celestine, respectively. Eq. 8 is also referred to as "solidus" equation. The corresponding aqueous solution composition is given by:

$$\Sigma \Pi = \left(\left[\text{Ba}^{2+} \right] + \left[\text{Sr}^{2+} \right] \right) \left[\text{SO}_4^{2-} \right]. \tag{9}$$

Squared brackets denote aqueous activities. With the aqueous mole fractions $X \left(\text{Ba}^{2+} \right)_{(\text{aq})} = \left[\text{Ba}^{2+} \right] / \left(\left[\text{Sr}^{2+} \right] + \left[\text{Ba}^{2+} \right] \right) = 1 - X \left(\text{Sr}^{2+} \right)_{(\text{aq})}$, Eqs. 8 and 9 can be rearranged to obtain the so called "solutus" equation (see Prieto 2009 for details):

$$\Sigma \Pi = 1 / \left[\left(X \left(\text{Ba}^{2+} \right)_{(\text{aq})} / \left(K_{\text{Ba}} f_{\text{Ba}} \right) \right) + \left(X \left(\text{Sr}^{2+} \right)_{(\text{aq})} / \left(K_{\text{Ce}} f_{\text{Ce}} \right) \right) \right]. \tag{10}$$

Plotting Eqs. 8 and 10 against 1. X_{Ba} and 2. $X(\text{Ba}^{2+})_{(\text{aq})}$ on the abscissa, a Lippmann Diagram is obtained (cf. Fig. 6). In this diagram, equilibrium solid and aqueous compositions are linked by horizontal lines (equal $\Sigma \Pi$). On the basis of Eqs. 8 and 10, it is further possible to construct a graph of $X(\text{Ba}^{2+})_{(\text{aq})}$ versus X_{Ba}, the so called Rozeboom diagram, an elegant way to relate aqueous composition with solid composition (cf. Fig. 5b). A local minimum in the solidus curve in the Lippmann diagram marks the beginning of a so called "spinodal gap" (marked with "SP" in Figs. 5b, 6). The beginning of the spinodal gap again marks a "peritectic point", which corresponds to an aqueous composition in equilibrium with two different solid compositions. Beyond the peritectic point there is a range of solid compositions, which are theoretically not achievable. Note that the beginning of the miscibility gap (1st local minimum in dG^{E}) and the beginning of the spinodal gap (1st local minimum in the solidus curve) do not coincide. Compositions inside the miscibility gap, but outside the spinodal gap are thought to be metastable (cf. Glynn 2000 or Bruno 2007). Nevertheless, one may think of kinetic controls on solid-solution formation, which may result in solid compositions, which should on the basis of thermodynamic considerations not be achievable (Shtukenberg et al. 2006) (i.e. inside the spinodal gap).

For statements on the formation of a solid-solution, it is of course most important to be able to quantify the saturation state of an aqueous solution with respect to the solid-solution. One way to do this is based on the so called stoichiometric solubility product, K_{st}, which is given by:

$$K_{\text{st}} = \left(K_{\text{Ba}} f_{\text{Ba}} X_{\text{Ba}} \right)^X * \left(K_{\text{Ce}} f_{\text{Ce}} X_{\text{Ce}} \right)^{(1-X)} = \left[\text{Ba}^{2+} \right]_{\text{eq}}^X \left[\text{Sr}^{2+} \right]_{\text{eq}}^{(1-X)} \left[\text{SO}_4^{2-} \right]_{\text{eq}}. \tag{11}$$

The index "eq" marks the aqueous activities in stoichiometric equilibrium with the solid-solution. It is important to note that the stoichiometric solubility marks no true thermodynamic equilibrium state, as it treats the solid-solution as a single component phase, which dissolves or precipitates congruently, i.e. with a given solid composition, $X = X_{\text{Ba}}$ (see Prieto 2009 for details). Nevertheless, Eq. 11 allows for a straightforward calculation of the saturation state of an aqueous solution with respect to a solid-solution of a given composition, the so called stoichiometric solubility product, Ω_{st}:

Heberling *et al. Geotherm Energy (2017) 5:9*

Page 6 of 16

$$\Omega_{\text{st}}(X) = \left[\text{Ba}^{2+}\right]^{X}\left[\text{Sr}^{2+}\right]^{(1-X)}\left[\text{SO}_4^{2-}\right]/K_{\text{st}}. \tag{12}$$

Note that in Eq. 12 the actual activities and not the stoichiometric equilibrium activities (index eq) are considered. According to Eq. 12, it is obvious that a solution with a given composition will have a range of supersaturations, depending on the solid composition, X. The solid composition, X_{max}, related to the highest supersaturation, Ω_{st} (X_{max}), coincides with the solid composition expected to form according to the Rozeboom diagram. Still, it is not necessarily the composition that will form (Prieto 2009).

Methods

Analytical methods

The scale sample was divided into three aliquots. One part was ground in an agate mortar and used for X-ray powder diffraction (XRPD) measurements. XRPD is performed in a Bruker D8 advance diffractometer. Due to the radioactivity of the sample, we measure XRPD in an air tight PMMA dome sample cell (Bruker A100B37). Diffractograms are analysed by means of Rietveld refinement using the Bruker Topas 4.2 software. The second part of the sample was kept intact and used for imaging the surface in a FEI Quanta 650 FEG environmental scanning electron microscope (ESEM). A third aliquot of the sample was embedded in epoxy resin, cut, polished, and used for element mapping performed by energy-dispersive X-ray fluorescence measurements (SEM–EDX, FEI Quanta 650 FEG).

Modelling

As already mentioned, we use PhreeqC 3 (Parkhurst and Appelo 2013) to model aqueous activities of $[\text{Ba}^{2+}]$, $[\text{Sr}^{2+}]$, and $[\text{SO}_4^{2-}]$, and the solubility products of the endmember phases, barite, and celestine. Calculations are performed assuming (1) 230 bar and 100 °C (reservoir conditions), (2) 1 bar and 70 °C (geothermal plant conditions), and (3) 1 bar and 25 °C (standard conditions). Where applicable, we compare results obtained with the ThermoChimie (SIT.dat Giffaut et al. 2014) and Pitzer [Pitzer.dat (Appelo et al. 2014)] databases. Solid-solution thermodynamic calculations are performed on the basis of aqueous activities and endmember solubilities from PhreeqC, using MS-Excel or a homemade Python code. In order to apply the mixing model by Becker et al. (2000) at the temperatures relevant to this study, we use the interaction parameters provided in Prieto et al. (Prieto et al. 2000) for 25 °C and adjust them to match the $\text{d}G^{\text{M}}(X)$ curves presented for various temperatures in Figure 5 in Becker et al. (2000). For comparison, we also apply a regular solid-solution model with $a_0 = 1.6$ (Monnin and Cividini 2006), or an ideal model.

Results and discussion

Sample characteristics

An SEM micrograph of the intact scaling surface is shown in Fig. 1. In the backscattered electron image, the lamellar $(\text{Ba,Sr})\text{SO}_4$ crystals appear in grey, while the dense, close to idiomorphic Galena (PbS) crystals appear in light grey.
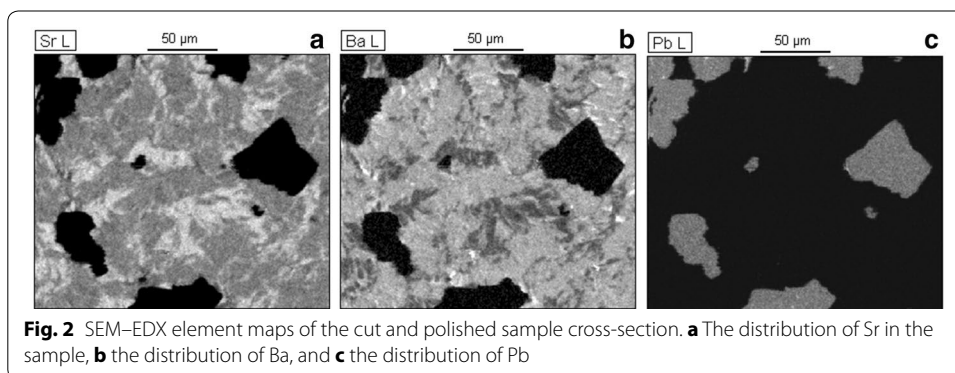
SEM–EDX element maps of the cut and polished sample cross-section are displayed in Fig. 2. The Sr- and Ba distribution (Fig. 2a, b), nicely show the heterogeneity in the (Ba,Sr)

Heberling *et al. Geotherm Energy* (2017) 5:9

Page 7 of 16

Fig. 1 Backscattered electron SEM micrograph of the intact scaling surface. Lamellar (Ba,Sr)SO_4 crystals appear in *grey*, the close to idiomorphic Galena (PbS) crystals appear in *light grey*
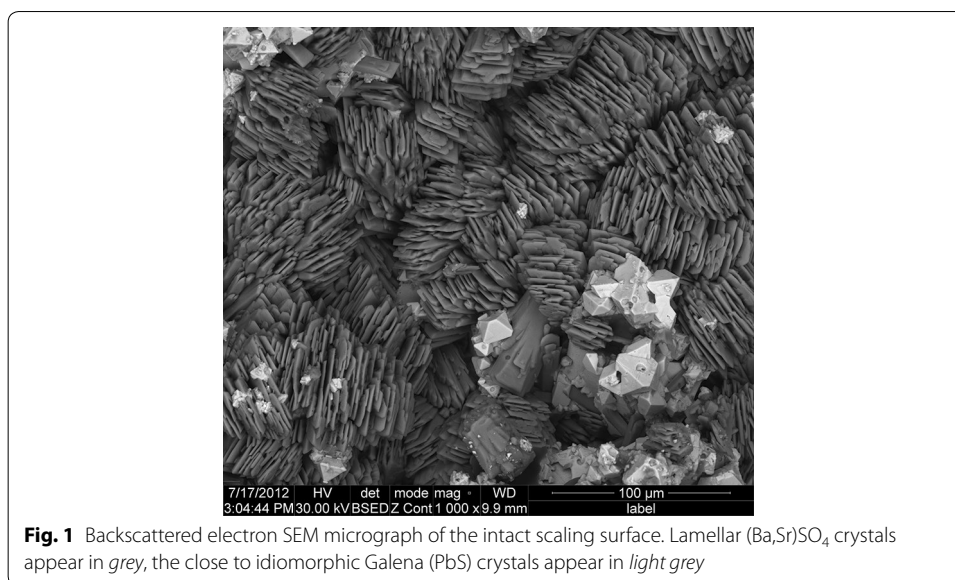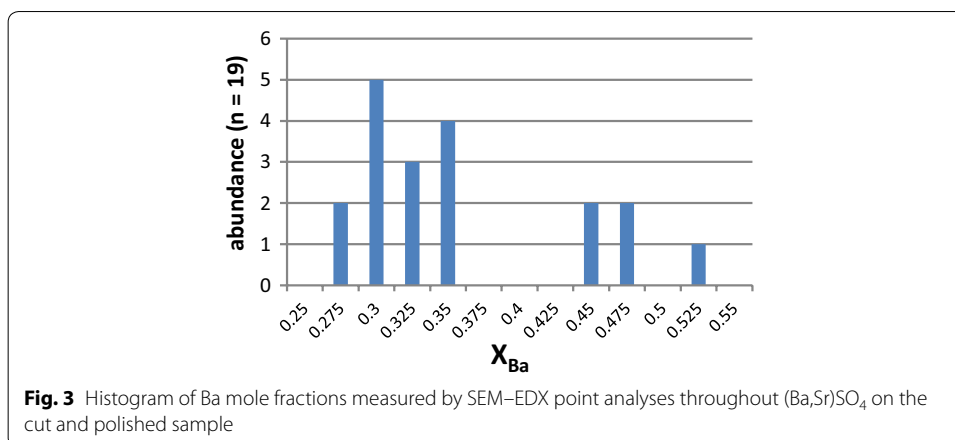
SO_4 compositions and the anti-correlation between the two elements. Thus, Sr-rich areas are poor in Ba and vice versa. It is also interesting to note the behaviour of Pb in the system (right image in Fig. 2). Though Pb^{2+} forms a sulphate mineral (anglesite) which is isostructural and to some extent miscible with barite (Glynn 2000), it is not detectable in the sulphate phase. Instead, Pb is fully gathered in the sulphide mineral galena. Obviously, due to the extremely low solubility of PbS [$\log_{10}(K_{SP}(\text{Galena})) = -31.94$, for the formation from Pb^{2+} and S^{2-} at 25 °C (Giffaut et al. 2014)], traces of S^{2-} are sufficient to bind Pb^{2+} quantitatively to the sulphide phase.

To further analyse the (Ba,Sr)SO_4 composition, we performed 19 point analyses throughout the (Ba,Sr)SO_4-dominated area of the cut and polished sample. The resulting X_{Ba} are depicted in a histogram in Fig. 3. We find a few spots with elevated Ba content around 50%, below there appears to be a gap, and the majority of points has a Ba content of 35% and lower.
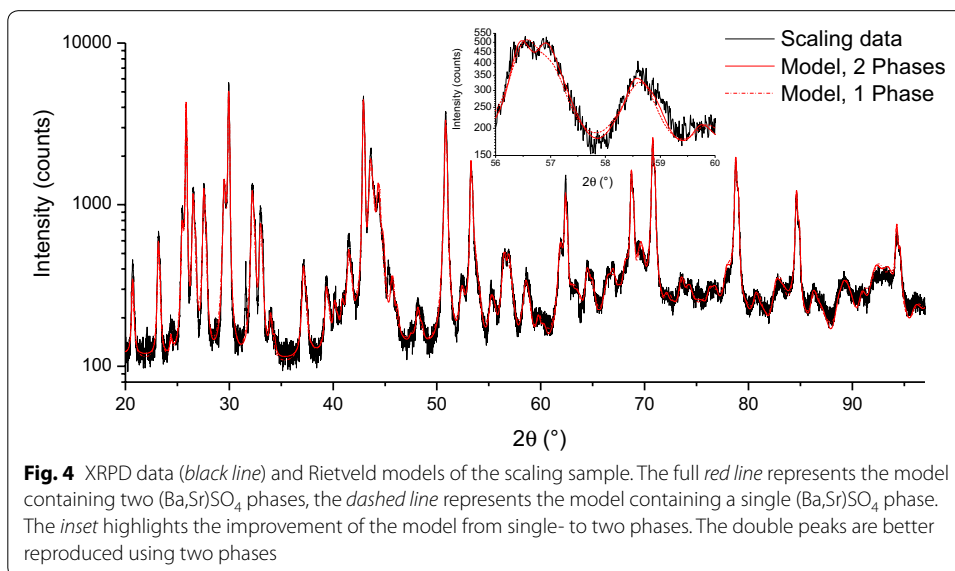
A powder diffractogram (black line) and corresponding Rietveld models (full- and dashed red lines) are shown in Fig. 4. The sharp reflexes in the diffractogram are related to cubic galena crystals, which represent about 19% of the sample. The composition of (Ba,Sr)SO_4 affects the model in two ways. First, the lengths of the unit cell axes vary,

Fig. 2 SEM–EDX element maps of the cut and polished sample cross-section. **a** The distribution of Sr in the sample, **b** the distribution of Ba, and **c** the distribution of Pb

Heberling *et al. Geotherm Energy* (2017) 5:9

Page 8 of 16

Fig. 3 Histogram of Ba mole fractions measured by SEM–EDX point analyses throughout (Ba,Sr)SO$_4$ on the cut and polished sample

according to Vegard's law, linearly with composition. This is in line with theoretical results (Becker et al. 2000), which did not indicate an excess mixing volume. Thus, the peak positions shift with composition. Second, the electron density at the cation sites varies with the composition, which influences the structure factors, i.e. the peak heights. The two effects are mathematically coupled in the Rietveld model, in order to minimize the number of adjustable parameters.

The Rietveld fit improved significantly (R_{wp} decreased from 12.3 to 10.5), when two instead of one (Ba,Sr)SO$_4$ phases are introduced into the model. This is highlighted in the insert in Fig. 4. The dashed line represents the one phase model. The full line depicting the two phase model reproduces the pronounced double peaks significantly better. Thus, the XRPD data clearly reflect the heterogeneous nature of the (Ba,Sr)SO$_4$ solid-solution. According to XRPD, the main phase of (Ba,Sr)SO$_4$ (about 56% of the sample) contains 32% barite ($X_{Ba} = 0.32$), which compares nicely to the majority of sample points from SEM–EDX. The second portion of (Ba,Sr)SO$_4$ represents 25% of the sample and contains about 15% Ba ($X_{Ba} = 0.15$).

Fig. 4 XRPD data (*black line*) and Rietveld models of the scaling sample. The full *red line* represents the model containing two (Ba,Sr)SO$_4$ phases, the *dashed line* represents the model containing a single (Ba,Sr)SO$_4$ phase. The *inset* highlights the improvement of the model from single- to two phases. The double peaks are better reproduced using two phases

Heberling *et al. Geotherm Energy* (2017) 5:9

Page 9 of 16

This second phase seems not to be present in the sample area of the SEM–EDX analyses. However, XRPD is a bulk analysis, while SEM–EDX probes merely an arbitrary small sample spot. Thus, we conclude that the bulk composition contains a significant amount of low barium $(Ba,Sr)SO_4$ ($X_{Ba} \approx 0.15$). The two analyses agree with respect to the main phase of $(Ba,Sr)SO_4$, with $X_{Ba} \approx 0.32$. Spots of high barium $(Ba,Sr)SO_4$ (up to $X_{Ba} = 0.53$) are identified in the SEM–EDX analysis. These, however, do obviously not contribute significantly to the bulk composition.

Besides the main elements (Ba, Sr, Pb, S, and O), the sample contained according to SEM–EDX Calcium, which is contained as a minor component in the sulphate phase, as well as traces of iron, and NaCl. Besides Galena and $(Ba,Sr)SO_4$, no further mineral phases were identified, like e.g. carbonates as they are frequently encountered in geothermal sites from the southern German Molasse Basin.

This scaling sample is particularly interesting for the present study, because it shows a whole range of $(Ba,Sr)SO_4$ compositions, which obviously may precipitate from aqueous solution at about 70 °C. At the same time, the solution composition of the geothermal brine in Neustadt-Glewe is well characterized [cf. Additional file 1: Table S1; (Degering et al. 2009)]. This provides optimal conditions to test which thermodynamic model is best suited to explain the observed solid compositions.

Modelling

The PhreeqC modelling results, i.e. the starting values for the solid-solution thermodynamic calculations, are reported in Table 1. The comparison of databases reveals first complications related to geochemical modelling of scale formation. Due to the high ionic strength of the brine (4.0 mol/kgw; kgw = kg water), it is clear that an approach like the specific ion interaction theory (SIT) (Ciavatta 1980) or Pitzer (1973) needs to be applied in order to accurately reproduce the activities of ions in solution. Fortunately, PhreeqC holds database files to simply apply both approaches. PhreeqC 3 corrects the solubility

Table 1 PhreeqC 3 modelling results: aqueous activities, solubility products (K_{SP}), and saturation indices (SI)

	$[Ba^{2+}]$ (mol/kgw)	$[Sr^{2+}]$ (mol/kgw)	$[SO_4^{2-}]$ (mol/kgw)	$\log_{10}(K_{SP})$: barite	$\log_{10}(K_{SP})$: celestine	SI[a] barite	SI celestine
Molalities	3.86 E−5	5.14E−3	4.89E−3	–	–	–	–
Pitzer: 230 bar, 100 °C	*8.35E−6*	*2.12E−3*	*4.10E−5*	*−9.36*	*−7.02*	*−0.11*	*−0.04*
Pitzer: 1 bar, 70 °C	*1.09E−5*	*2.57E−3*	*5.00E−5*	*−9.54*	*−6.93*	0.28	0.04
Pitzer: 1 bar, 25 °C	*1.91E−5*	*3.36E−3*	*5.35E−5*	*−9.84*	*−6.66*	0.85	−0.09
Pitzer: 1 bar, 25 °C (no ana.-expr.)	*1.91E−5*	*3.36E−3*	*5.35E−5*	*−9.97*	*−6.63*	0.98	−0.12
SIT: 1 bar, 25 °C	6.62E−6	2.74E−4 (1.54E−3, incl. SrCl+)	1.24E−4	−9.97	−6.62	0.88	−0.85 (−0.10, incl. SrCl+)

The values highlighted in italics are those considered in solid-solution thermodynamic calculations
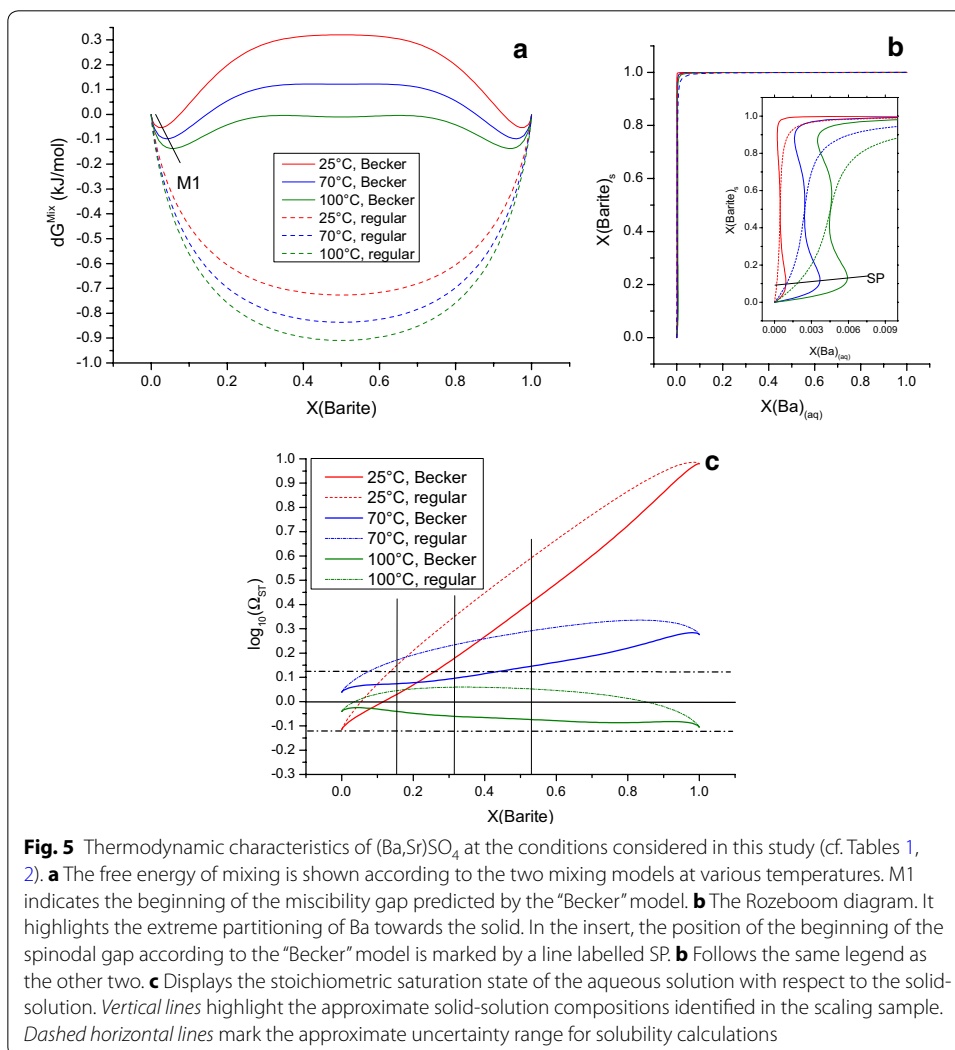
kgw kg water

[a] $SI = \log_{10}([Me^{2+}][SO_4^{2-}]/K_{SP})$

products for temperature effects by an empirical relation (termed analytical expression in PhreeqC; ana.-expr. In Table 1). Both, SIT- and Pitzer database contain parameters needed to calculate the solubility of barite and celestine as a function of temperature. Only the Pitzer database contains parameters needed to correct the solubility for pressure effects. A look into the original literature reveals that the parameters for temperature correction in SIT.dat are only valid up to 40 °C (Langmuir and Melchior 1985). Thus this database is not applicable for the present case. Comparison between SIT.dat and Pitzer.dat reveals that the use of SIT.dat for calculations of barite and celestine solubility at higher temperatures would lead to severe errors: 0.5 log units at 100 °C and 1.7 log units at 200 °C. Furthermore, according to SIT.dat, Sr^{2+} speciation is dominated by a $SrCl^+$ complex for Sr^{2+} at high Cl^- concentrations, which leads to an underestimation of the celestine saturation (indicated in the last line in Table 1). On the other hand side, the analytical expression parameters reported in SIT.dat correctly reproduce the standard values for barite and celestine solubility at 25 °C, $\log_{10}(K_{SP}) = -9.97$ and -6.63, respectively. This points to an inconsistency in Pitzer.dat. While the Pitzer database lists the same standard values for barite and celestine solubility, the analytical expression parameters produce values of $\log_{10}(K_{SP}) = -9.84$ and -6.66 for barite and celestine at standard conditions, respectively. This seems to characterize the range of uncertainty one has to deal with, when modelling solubility at various temperatures. The analytical expression parameters and pressure corrections used for barite and celestine in Pitzer.dat are valid up to >200 °C, and 1000 bar (Monnin 1999; Blount 1977; Appelo et al. 2014). In this study, we decided to rely on the calculations with Pitzer.dat. However, at room temperature, we use the standard values for barite and celestine solubility instead of those calculated by the analytical expression.
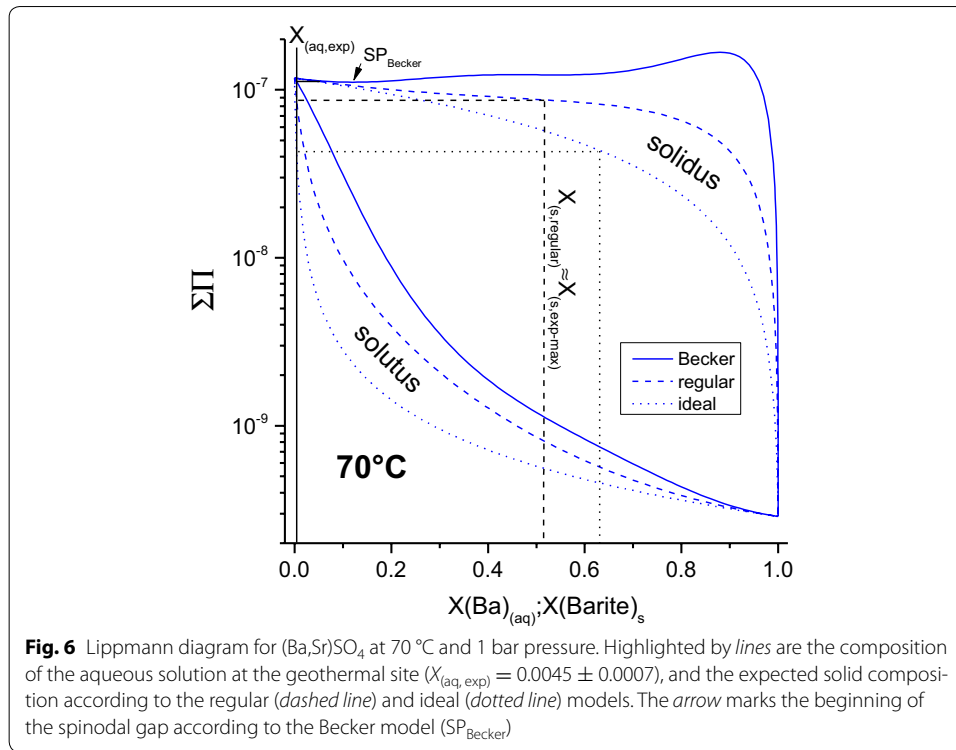
The solution pH is set to 5.15 at reservoir conditions (Kühn et al. 1997). According to calculations with the Pitzer database, pH increases upon a decrease of pressure and temperature to pH 5.9 at geothermal plant conditions and to pH 7.0 at standard conditions. All other changes in speciation are minor. The increase of the supersaturation with respect to barite and celestine is dominated by the effect of pressure and temperature on the solubility products.

We apply various solid-solution mixing models for comparison. Those based on the theoretical work by Becker et al. (2000) and Prieto et al. (2000) are in the following termed "Becker" model, they are compared to calculations using a "regular", and in case an ideal model (involving no interaction parameters). The interaction parameters used to model the mixing of $(Ba,Sr)SO_4$, as displayed in Figs. 5, 6, are listed in Table 2. Figure 5a displays the free energy of mixing. It demonstrates the pronounced miscibility gap predicted by the Becker model (starting at the point marked: M1), which ranges from 2 to 98% barite at 25 °C and reduces to 6–94% barite at 100 °C. The regular model on the other hand predicts complete mixing. The Rozeboom diagram, displayed in Fig. 5b, highlights the extreme partitioning of Ba towards the solid phase. This is an effect of the pronounced difference between the solubility products of the endmember phases of 2.3 (100 °C) to 3.3 (25 °C) log units depending on temperature. Only in the magnification (insert in Fig. 5b), the variations with temperature and mixing model become visible. As a consequence of the miscibility gap, the Rozeboom diagram predicts a spinodal gap for the Becker model (starting at the point marked SP in Fig. 5).

Heberling *et al. Geotherm Energy (2017) 5:9*

Page 11 of 16

Fig. 5 Thermodynamic characteristics of $(Ba,Sr)SO_4$ at the conditions considered in this study (cf. Tables 1, 2). **a** The free energy of mixing is shown according to the two mixing models at various temperatures. M1 indicates the beginning of the miscibility gap predicted by the "Becker" model. **b** The Rozeboom diagram. It highlights the extreme partitioning of Ba towards the solid. In the insert, the position of the beginning of the spinodal gap according to the "Becker" model is marked by a line labelled SP. **b** Follows the same legend as the other two. **c** Displays the stoichiometric saturation state of the aqueous solution with respect to the solid-solution. *Vertical lines* highlight the approximate solid-solution compositions identified in the scaling sample. *Dashed horizontal lines* mark the approximate uncertainty range for solubility calculations

The stoichiometric supersaturation of the aqueous solution with respect to the solid-solution is depicted in Fig. 5c. It shows that the solution composition agrees well with the aqueous solution being at equilibrium with $(Ba,Sr)SO_4$ at reservoir conditions (100 °C, 230 bar). At geothermal plant conditions (70 °C, 1 bar), the aqueous solution is, according to the Becker model, still not significantly supersaturated with respect to the identified solid-solution compositions. According to the regular model the supersaturation is about a factor of two higher in the relevant composition range, but still not very pronounced ($\log_{10}(\Omega_{ST}) < 0.3$). This corresponds nicely to the study by Kühn et al. (1997), who observed neither homogeneous nor heterogeneous nucleation of a $(Ba,Sr)SO_4$ scaling at these conditions within the time frame of their experiments. Upon further reduction of temperature, the supersaturation especially with respect to high barium $(Ba,Sr)SO_4$ becomes more pronounced.

The most complete depiction of the relation between aqueous- and solid-solution compositions is the Lippmann diagram. It is shown in Fig. 6 for geothermal plant conditions. The composition of the aqueous solution is marked by a vertical line labelled $X_{(aq, exp)}$

Heberling *et al. Geotherm Energy (2017) 5:9*

Page 12 of 16

Fig. 6 Lippmann diagram for (Ba,Sr)SO$_4$ at 70 °C and 1 bar pressure. Highlighted by *lines* are the composition of the aqueous solution at the geothermal site ($X_{(aq, exp)} = 0.0045 \pm 0.0007$), and the expected solid composition according to the regular (*dashed line*) and ideal (*dotted line*) models. The *arrow* marks the beginning of the spinodal gap according to the Becker model (SP$_{Becker}$)

Table 2 Interaction parameters used to model solid-solution mixing in this study

	Becker, 25 °C	Becker, 70 °C	Becker, 100 °C	Regular (all temperatures)
a_0	3.28	2.94	2.76	1.6
a_2	1.11	1.00	0.93	–
a_4	−0.48	−0.43	−0.40	–

(=0.0045 ± 0.0007). The intersection points of this line with the solutus curves mark the $\Sigma\Pi$ values, which tie the aqueous composition with the solid composition read from the solidus curve. These are the compositions expected to form according to thermodynamics. As mentioned before, the Becker model predicts a spinodal gap. According to this model, all solid compositions identified in the scaling sample would reflect non-equilibrium partitioning. Thus, if this model was correct, solid-solution precipitation in the geothermal plant would be fully kinetically controlled. This may not be considered impossible, but it would mean a huge draw back for all attempts to describe scale formation using thermodynamic models. Furthermore, in the supersaturation range, we are faced with at the conditions in this geothermal plant ($\log_{10}(\Omega_{ST}) < 0.35$, cf. blue curves in the right graph in Fig. 5), pronounced kinetic effects would be unexpected.

The regular model represents the scenario best suited to describe the observed scaling compositions. The expected composition of the solid ($X_{Ba} = 0.55 \pm 0.08$) coincides with the maximal Ba content, identified in the SEM–EDX analysis. Thermodynamics predict a strong partitioning of Ba towards the solid. Thus, any precipitation of (Ba,Sr)SO$_4$ before the location where the scaling sample was precipitated, would efficiently deplete the brine, which is anyway poor in Ba^{2+} ($X(Ba)_{(aq)} = 0.0045$), further with respect to

Heberling *et al. Geotherm Energy* (2017) 5:9

Page 13 of 16

Ba^{2+}. A reduction of $X(Ba)_{(aq)}$ about a factor of 2.6 (to 0.0017) would suffice to explain the lowest Ba content identified in the scaling sample, $X_{Ba} = 0.15$. According to the ideal model (dotted line in Fig. 6), higher Ba content in the solid would be expected and stronger fluctuations in $X(Ba)_{(aq)}$ (about a factor of 10) would be necessary to explain the observed heterogeneity of the solid.

One might be tempted to consider the observed X_{Ba} values (Fig. 3) as an indication for a spinodal gap around $X_{Ba} = 0.4$. This is, however, not in line with any possible choice of the interaction parameter.

Thus, a regular solid-solution model with $a_0 = 1.6$ as previously proposed by Monnin and Cividini (2006) is considered a good choice to describe our observations. Note that our results do not strongly constrain the interaction parameter. Any value $1.5 < a_0 < 1.8$ would be in line with the observations. Monnin and Cividini suggested their value for $(Ba,Sr)SO_4$ formation in ocean waters at lower temperature (<5 °C). In principle, a decrease of the interaction parameters with increasing temperature, as we derived it for the values from the Becker model, seems very plausible, as it reflects a decrease of structural strain with increasing molecular motion. Thus, our results are somewhat contradictory to the suggestion by Monnin and Cividini, because if the interaction parameter was 1.6 at 70 °C it should be significantly higher at 5 °C, or vice versa.

The heterogeneity in the scaling sample can be explained by any small variations in $X(Ba)_{(aq)}$, which have according to thermodynamics a strong effect on X_{Ba}. A similar effect has previously been described as bimodal precipitation of $(Ba,Sr)SO_4$ and leads to pronounced zoning in natural or synthetic $(Ba,Sr)SO_4$ crystals (Prieto et al. 1997). Thus varying solid compositions could reflect varying flow conditions in the pipes, which lead to varying degrees of $(Ba,Sr)SO_4$ precipitation before the location of the scaling. Previous studies suggest that the scaling was deposited continuously over a period of 4 years (Degering et al. 2009). Fluctuations in the composition of the brine during this period, which were not covered by the fluid sampling in (Degering et al. 2009), could as well explain the scaling heterogeneity. Another scenario to explain the composition of the scaling, which we consider quite likely, would be that $(Ba,Sr)SO_4$ scalings form with decreasing barium content along the flow path of the brine in the geothermal plant, along with a continuous depletion of the brine with respect to barium. The final heterogeneous scaling might then form as a consequence of transport, mixing, and deposition of preformed solid particles.

Concerning the recently discussed recrystallization of barite type solid-solutions, which may lead to a homogenization of the solid within months or years at stagnant solution conditions (Curti et al. 2010; Brandt et al. 2015), we may conclude that similar processes do not significantly affect geothermal scales at the flow conditions as encountered at the geothermal site considered in this study (Seibt et al. 2005), otherwise a homogenization of the $(Ba,Sr)SO_4$ composition would be expected.

Conclusions

The investigated scaling sample consists of 19% Galena and of 81% of a $(Ba,Sr)SO_4$ solid-solution with a very heterogeneous composition, which ranges from $0.15 < X_{Ba} < 0.53$. A main fraction of the sample (~56%) has a Ba content of $X_{Ba} \approx 0.32$. The rest (~25%) is dominated by $(Ba,Sr)SO_4$ with lower Ba content, $X_{Ba} \approx 0.15$.

Heberling *et al. Geotherm Energy* (2017) 5:9

Page 14 of 16

We note that considerable uncertainties are related to the description of $(Ba,Sr)SO_4$ formation by means of thermodynamic models. The scaling composition observed in this study would be in line with endmember solubilities as predicted by the PhreeqC-Pitzer database for 70 °C and a regular solid-solution model with an interaction parameter, $a_0 = 1.6$. At the current state of knowledge and on the basis of this study, we recommend the use of such a simple model to describe $(Ba,Sr)SO_4$ compositions after precipitation from aqueous solution. According to such a model, the scaling heterogeneity reflects bimodal precipitation behaviour due to various degrees of depletion of the brine with respect to $X(Ba)_{(aq)}$. Minor fluctuations in $X(Ba)_{(aq)}$: $0.0017 < X(Ba)_{(aq)} < 0.0045$ explain the full range of observed solid compositions.

However, the choice of the mixing parameter seems to some extent arbitrary. This knowledge gap strongly limits the interpretation of $(Ba,Sr)SO_4$ compositions based on thermodynamic models. Thus, it is not strictly possible to distinguish between kinetic and thermodynamic effects on partitioning. It is our impression that sound values for the $(Ba,Sr)SO_4$ mixing parameters as a function of temperature could deliver valuable information about scale formation processes. E.g. in the present range of solution compositions, temperature changes would have an extreme effect on the solid composition. Thus, $(Ba,Sr)SO_4$ compositions could be used as a very sensitive geothermometer. Considering the experimental difficulties related to $(Ba,Sr)SO_4$ formation from aqueous solution, especially a renewed assessment of the interaction parameters based on atomistic simulations [e.g. using DFT (Vinograd et al. 2013)] seems desirable.

Additional file

Additional file 1: Figure S1. Geologic map of Mecklenburg-Vorpommern showing pre-quaternary formations. Highlighted with a blue triangle is the location of the geothermal site near Neustadt-Glewe. The map was downloaded from Environmental Geodata Services Mecklenburg-Vorpommern at: http://www.umweltkarten. mv-regierung.de/atlas. For more detailed information about the geothermal usability of the underground in Mecklenburg-Vorpommern, but also in Germany in general, we refer the reader to a brochure published by LIAG, which is available at: https://geotis.de/homepage/Ergebnisse/LIAG_Broschuere_Tiefe_Geothermie.pdf and contains a number of very informative maps. **Table S1.** Composition of the geothermal brine from Neustadt-Glewe (after ref. (Degering et al. 2009) from the main manuscript). For comparison the composition used for modelling (after ref. (Kühn et al. 1997) from the main manuscript) is given in the last column.

Author details
[1] Institute for Nuclear Waste Disposal, Karlsruhe Institute of Technology, PO Box 3640, 76021 Karlsruhe, Germany. [2] VKTA-Strahlenschutz, Analytik & Entsorgung Rossendorf e. V., PO Box 510119, 01314 Dresden, Germany.

Competing interests
We declare neither competing financial interests nor any other competing interests.

Availability of data and materials
All information and data necessary to follow the interpretations and conclusions drawn in the present manuscript are presented in the main text in tables and figures or can be found in cited references.

Heberling *et al. Geotherm Energy* (2017) 5:9

Page 15 of 16

Publisher's Note

Springer Nature remains neutral with regard to jurisdictional claims in published maps and institutional affiliations.

References

Appelo CAJ, Parkhurst DL, Post VEA. Equations for calculating hydrogeochemical reactions of minerals and gases such as CO_2 at high pressures and temperatures. Geochim Cosmochim Acta. 2014;125:49–67.

Becker U, Fernandez-Gonzalez A, Prieto M, Harrison R, Putnis A. Direct calculation of thermodynamic properties of the barite/celestine solid solution from molecular principles. Phys Chem Miner. 2000;27(4):291–300.

Blount C. Barite solubilities and thermodynamic quantities up to 300 °C and 1400 bars. Am Miner. 1977;62:942–57.

Brandt F, Curti E, Klinkenberg M, Rozov K, Bosbach D. Replacement of barite by a $(Ba,Ra)SO_4$ solid solution at close-to-equilibrium conditions: a combined experimental and theoretical study. Geochim Cosmochim Acta. 2015;155:1–15.

Bruno J. Chemical thermodynamics of solid solutions of interest in radioactive waste management: a state-of-the-art report. London: OECD Publishing; 2007.

Ciavatta L. The specific interaction theory in evaluating ionic equilibria. Anal Chim. 1980;70:551–67.

Curti E, Fujiwara K, Iijima K, Tits J, Cuesta C, Kitamura A, Glaus MA, Muller W. Radium uptake during barite recrystallization at 23 ± 2 °C as a function of solution composition: an experimental Ba-133 and Ra-226 tracer study. Geochim Cosmochim Acta. 2010;74(12):3553–70.

Degering D, Köhler M, Friedrich H. Verbundvorhaben: Langfristige Betriebssicherheit geothermischer Anlagen–Teilprojekt: Mobilisierung und Ablagerungsprozesse natürlicher Radionuklide; report 2009. doi: 10.2314/GBV:617432368.

Degering D, Köhler M, Hielscher M. Vorkommen und Verhalten Natürlicher Radionuklide im Aquifer, im Fluid und in den Ablagerungen der Geothemieanlage Neustdt-Glewe. Z Geol Wiss. 2011;39(3/4):275–90.

Felmy AR, Rai D, Moore DA. The solubility of $(Ba,Sr)SO_4$ precipitates: thermodynamic equilibrium and reaction path analysis. Geochim Cosmochim Acta. 1993;57(18):4345–63.

Giffaut E, Grivé M, Blanc P, Vieillard P, Colàs E, Gailhanou H, Gaboreau S, Marty N, Made B, Duro L. Andra thermodynamic database for performance assessment: thermoChimie. Appl Geochem. 2014;49:225–36.

Glynn PD. Solid-solution solubilities and thermodynamics: sulfates, carbonates, and halides. In: Alpers CN, Jambor JL, Nordstrom D, editors. Sulfate minerals: crystallography, geochemistry, and environmental significance, vol. 40. Chantilly: Mineralogical Society of America; 2000. p. 480–511.

Guggenheim EA. Theoretical basis of Raoult's law. Trans Faraday Soc. 1937;33:151–9.

IAEA extent of environmental contamination by naturally occurring radioactive material (norm) and technological options for mitigation; international atomic energy agency, technical report series 419, Vienna, 2003.

Jacobsen SD, Smyth JR, Swope RJ, Downs RT. Rigid-body character of the SO_4 groups in celestine, anglesite and barite. Can Miner. 1998;36:1053–60.

Kühn M, Frosch G, Kölling M, Kellner T, Althaus E, Schulz HD. Experimentelle Untersuchungen zur Barytübersättigung einer Thermalsole. Grundwasser. 1997;2(3):111–7.

Langmuir D, Melchior D. The geochemistry of Ca, Sr, Ba and Ra sulfates in some deep brines from the Palo Duro Basin, Texas. Geochim Cosmochim Acta. 1985;49(11):2423–32.

Monnin C. A thermodynamic model for the solubility of barite and celestine in electrolyte solutions and seawater to 200 °C and to 1 kbar. Chem Geol. 1999;153(1):187–209.

Monnin C, Cividini D. The saturation state of the world's ocean with respect to $(Ba,Sr)SO4$ solid solutions. Geochim Cosmochim Acta. 2006;70(13):3290–8.

Parkhurst DL, Appelo C. Description of input and examples for PHREEQC version 3—a computer program for speciation, batch-reaction, one-dimensional transport, and inverse geochemical calculations. Us Geol Survey Tech Methods. 2013;6:497.

Pitzer KS. Thermodynamics of electrolytes. I. Theoretical basis and general equations. J Phys Chem. 1973;77(2):268–77.

Prieto M. Thermodynamics of solid solution–aqueous solution systems. Rev Miner Geochem. 2009;70:47–85.

Prieto M, Fernández-González A, Putnis A, Fernández-Díaz L. Nucleation, growth, and zoning phenomena in crystallizing $(Ba,Sr)CO3$, $Ba(SO4, CrO4)$, $(Ba,Sr)SO4$, and $(Cd, Ca)CO_3$ solid solutions from aqueous solutions. Geochim Cosmochim Acta. 1997;61(16):3383–97.

Prieto M, Fernandez-Gonzalez A, Becker U, Putnis A. Computing Lippmann diagrams from direct calculation of mixing properties of solid solutions: application to the barite-celestine system. Aquat Geochem. 2000;6(2):133–46.

Prieto M, Heberling F, Rodríguez-Galán RM, Brandt F. Crystallization behavior of solid solutions from aqueous solutions: an environmental perspective. Prog Cryst Growth Charact Mater. 2016;62(3):29–68.

Seibt P, Kabus F, Hoth P. In: Proceedings word geothermal congress. The Neustadt-Glewe geothermal power plant–practical experience in the reinjection of cooled thermal waters into sandstone aquifers, Antalya. 2005.

Shtukenberg AG, Punin YO, Azimov P. Crystallization kinetics in binary solid solution–aqueous solution systems. Am J Sci. 2006;306(7):553–74.

Todd AC, Yuan M. Barium and strontium sulfate solid solution formation in relation to North Sea scaling problems. Soc Pet Eng. 1990. doi:10.2118/18200-PA.

Heberling *et al. Geotherm Energy* (2017) 5:9

Page 16 of 16

Todd AC, Yuan MD. Barium and strontium sulfate solid-solution scale formation at elevated temperatures. Soc Pet Eng. 1992. doi:10.2118/19762-PA.

Vinograd VL, Brandt F, Rozov K, Klinkenberg M, Refson K, Winkler B, Bosbach D. Solid–aqueous equilibrium in the $BaSO_4$–$RaSO_4$–H_2O system: first-principles calculations and a thermodynamic assessment. Geochim Cosmochim Acta. 2013;122:398–417.